Available online at www.sciencedirect.com
ScienceDirect
Catalysis Today 116 (2006) 469–477
CATALYSIS TODAY
www.elsevier.com/locate/cattod

Hydrodesulfurization of hindered dibenzothiophenes on bifunctional NiMo catalysts supported on zeolite–alumina composites

Dora Solís [a,c,*], Antonio López Agudo [b], Jorge Ramírez [a], Tatiana Klimova [a]

[a] *Facultad de Química, UNAM, Cd. Universitaria, Coyoacán, México D.F. 04510, Mexico*
[b] *Instituto de Catálisis y Petroleoquímica, CSIC, Cantoblanco, 28049 Madrid, Spain*
[c] *Facultad de Química, UAEM, Paseo Colón s/n, 50 000 Toluca, Mexico*

Available online 25 July 2006

Abstract

A series of NiMo catalysts supported on HNaY(x)–Al_2O_3 composites with different amounts of HNaY zeolite (x = 0, 5, 10, 20 and 100 wt.% of HNaY) was prepared and tested in the hydrodesulfurization (HDS) of dibenzothiophene (DBT) and 4,6-dimethyl-DBT (4,6-DMDBT). The catalysts were characterized by N_2 physisorption, X-ray diffraction (XRD), FT-IR spectroscopy of pyridine and nitrogen oxide adsorption (Py and NO-FT-IR), temperature-programmed reduction (TPR), scanning electron microscopy (SEM-EDX) and high-resolution transmission electron microscopy (HRTEM). It was found that the increase in the zeolite content causes changes in the acidic properties of the catalyst (number of acid sites) as well as in the characteristics of the deposited metallic species (location and dispersion). Different activity trends with the amount of the zeolite were found for the DBT and 4,6-DMDBT hydrodesulfurization on NiMo/HNaY-Al_2O_3 catalysts. As for the HDS of DBT the alumina-supported catalyst presents the highest activity. The incorporation of the zeolite causes an initial drop and then the recovery of activity with zeolite content. In contrast, for the 4,6-DMDBT the HDS activity always increases with zeolite content. These two different catalytic behaviors seem to be due to two opposite effects, which affect the contribution of the reaction routes available for the HDS of each reactant, these effects are: (i) the decrease of MoS_2 dispersion caused by the incorporation of zeolite to the catalyst and (ii) the increase of the proportion of Brönsted acid sites with zeolite content. The reaction product distribution indicates that both types of sites, coordinatively unsaturated sites (CUS) of the MoS_2 and zeolite Brönsted acid sites, participate in the 4,6-DMDBT and DBT transformations.

Keywords: Bifunctional catalyst; Brönsted acid sites; HNaY zeolite; Hydrodesulfurization; DBT; 4,6-DMDBT; NiMo catalyst

1. Introduction

Recently, the interest in new catalysts for deep hydrodesulfurization (HDS) has been growing due to the environmental restrictions that limit the sulfur content in gasoline and diesel fuels. Therefore, many efforts have been made to improve the design and the performance of new catalysts in order to reach high desulfurization activity towards strongly hindered sulfur-containing molecules such as dibenzothiophene (DBT) and its alkyl-substituted derivatives. Those compounds with alkyl groups in positions 4 and 6 of the DBT (4-MDBT and 4,6-dimethyl-DBT (4,6-DMDBT)) are particularly refractory towards HDS and cannot be adequately removed by using the current catalytic formulations (Co)NiMo/Al_2O_3 [1]. The reactivity of alkyl-substituted DBT's is almost six times smaller than that of the DBT due to the restricted access of the sulfur reactant molecule to the catalyst active sites, which is caused by the steric hindrance of the methyl groups [2,3]. It has been previously reported that the DBT and 4,6-DMDBT undergo HDS via two reaction pathways [2–4]: (1) direct desulfurization (DDS), which leads to the formation of biphenyls; (2) hydrogenation (HYD) yielding tetrahydro- and hexahydro-intermediates followed by desulfurization to cyclohexylbenzenes and bicyclohexyls. The DBT is converted predominantly via the DDS pathway, whereas 4,6-DMDBT reacts mainly via the HYD pathway. It is well known that the hydrogenation of the 4,6-DMDBT molecule prior to sulfur removal alleviates the steric hindrance and, therefore, facilitates the HDS reaction [3–7]. Another possibility to increase the desulfurization of the 4,6-DMDBT is to add an acid function to the conventional catalyst [3–14], obtaining a bifunctional catalyst, which should promote the DDS, HYD, alkylation (ALK), cracking (CKG) and

* Corresponding author. Fax: +52 55 56 22 53 71.
E-mail address: solis_casados@yahoo.com.mx (D. Solís).

0920-5861/$ – see front matter © 2006 Elsevier B.V. All rights reserved.
doi:10.1016/j.cattod.2006.06.029

isomerization (ISO) of the reactive molecule. Landau et al. [7] reported the incorporation of HY or HZSM-5 zeolites into the conventional CoMo catalyst and found that although other reaction routes are promoted, the catalysts containing zeolite were deactivated at high rate as a result of coke deposition provoked by strong Brönsted acid sites. Apparently, in this case, the amount of zeolite incorporated to the catalyst was too high. Kunisada et al. [8] reported the addition of 50 wt.% of a strong acid function (USY zeolite) to a $NiMo/Al_2O_3$ catalyst for the HDS of gasoil (SRGO). They found enhanced HDS and HYD activities but also some cracking that diminished when the reaction temperature was lowered from 340 to 320 °C. In the past we reported that the incorporation method of the HNaY zeolite to the conventional catalyst affects the coordination state, the location and dispersion of the metallic species as well as the number of available acid sites [13]. These changes affected the catalytic performance and the ratio of reaction routes, evidenced by different product distributions. Cid et al. [14] reported on the use of Ni exchanged NaY zeolite, obtaining a better dispersion of the metallic phase and a better HDS catalytic activity than with the HNaY zeolite. We have already reported before the effect of the zeolite content in $NiMo/Al_2O_3$–zeolite mechanical mixtures [15]. HNaY and Ni exchanged zeolite were used. A better catalytic performance was observed in HDS of prehydrotreated than of untreated gasoil. The lower HDS activity of the HNaY and $NiMo/HNaY\text{-}Al_2O_3$ was attributed to the rapid deactivation of the acid sites of HNaY by coke formation. According to the aforementioned, it is clear that the performance of a NiMo/alumina-zeolite HDS catalyst should be also affected by the amount of zeolite, since this will alter the balance of the different catalyst functionalities (provided by sulfided metallic and acidic sites). However, the study of this effect has not been properly addressed in the literature.

The objective of this study was to investigate how the incorporation of different amounts of zeolite HNaY into an alumina matrix and then its further use as a support influences the structure and catalytic properties of the $NiMo/HNaY\text{-}Al_2O_3$ catalysts in the HDS of the DBT and 4,6-DMDBT. Consideration was also given to the location and dispersion of the Mo and Ni phases deposited over these supports. For this aim, a series of $NiMo/Al_2O_3$-HNaY catalysts with zeolite contents of 5, 10, 20 and 100 wt.% zeolite were prepared and tested in the HDS of DBT and 4,6-DMDBT. The catalysts were characterized by N_2 physisorption, X-ray powder diffraction (XRD), nitrogen oxide (NO) and pyridine (Py)-IR spectroscopy, temperature-programmed reduction (TPR), scanning electron microscopy (SEM-EDX) and high-resolution transmission electron microscopy (HRTEM).

2. Experimental

2.1. Support and catalyst preparation

A series of NiMo catalysts was supported on $HNaY(x)$–Al_2O_3 composites containing different zeolite loadings ($x = 0$, 5 10, 20 and 100 wt.%). The starting materials for the preparation of the $HNaY(x)\text{-}Al_2O_3$ supports were a commercially available NaY zeolite (Si/Al ratio = 2.42) and pseudoboehmite Catapal B. Firstly before use, the NaY (faujasite) zeolite was 58% exchanged with an ammonium acetate solution to obtain HNaY. Different amounts of this zeolite were incorporated into an alumina matrix by using diluted formic acid as peptizing agent. The level of partial dealumination occurring during the formation of Al_2O_3–zeolite composites with different zeolite contents has been reported in a previous work [16]. In our case, the pH of the mixture was maintained above 3 to minimize zeolite dealumination. The impregnation of Ni and Mo (Mo first) on the $HNaY(x)\text{-}Al_2O_3$ supports was made by incipient wetness method by using aqueous solutions of nickel nitrate and ammonium heptamolybdate as precursors. After each impregnation, the catalysts were dried (100 °C, 24 h) and calcined (500 °C for 2 h). The nominal composition of the catalysts was 12 wt.% MoO_3 and 3 wt.% NiO.

2.2. Characterization

N_2 adsorption–desorption isotherms were obtained at liquid-N_2 temperature by using a Micromeritics ASAP 2000 automatic analyzer. Prior to the experiments, the samples were degassed ($P < 10^{-1}$ Pa) at 250 °C for 3 h. Specific surface areas were calculated by the BET method (S_{BET}), the pore volume (V_p) was determined by N_2 adsorption at a relative pressure of 0.98 and pore size distributions (D_p) determined for a maximum of desorption pore size distribution curves from the BJH method. The microporous area (S_μ) was estimated by using the *t*-plot method.

The X-ray diffraction patterns were recorded in the range $3^\circ \leq 2\theta \leq 80^\circ$ in a Philips PW 1050/25 diffractometer using Fe-filtered Cu Kα radiation (λ = 1.5418 Å) and a goniometer speed of 1° (2θ) min^{-1}.

FT-IR measurements were performed with a Nicolet 510 spectrometer. The IR spectra were recorded at room temperature, with 300 scans and 4 cm^{-1} resolution. The pyridine adsorption was performed on oxided samples at room temperature and measured after evacuating at several temperatures ranging from room temperature to 400 °C. NO adsorptions were made on pre-sulfided samples at room temperature. TPR experiments were performed in an automated ISRI-RIG-100 characterization system equipped with a TCD. Before the analysis the samples were pretreated at 500 °C for 2 h under air flow and cooled in an Ar stream in order to remove water and other contaminants. The reduction step was performed with an H_2/Ar mixture, with a heating rate of 10 °C/min, from room temperature to 1000 °C. SEM-EDX profiles were obtained by using a JEOL 5900 LV microscope equipped with Oxford ISIS chemical analysis system.

High-resolution transmission electron microscopy characterizations of sulfided catalysts were performed using a JEOL 2010 microscope (with a point-to-point resolution of 1.9 Å). The solids were ultrasonically dispersed in heptane and the suspension was deposited on carbon-coated copper grids.

2.3. Activity measurements

The catalysts were evaluated in the hydrodesulfurization of the DBT and 4,6-DMDBT in a 300 ml batch stirred reactor at 300 °C and with a total pressure of 7.3 MPa for 8 h. In each run the autoclave was charged with 0.15 g of catalyst and 40 ml of mixture containing 0.47 g of DBT (Aldrich, 98%) or 0.21 g of 4,6-DMDBT (Aldrich, 97%) dissolved in *n*-hexadecane (Sigma, 99%), which corresponds to 0.26 or 0.1 wt.% of S, respectively. The activation of the catalysts was made by ex situ sulfidation in a tubular reactor by a 15 vol.% H_2S/H_2 flow at 400 °C for 4 h. The course of the reaction was followed by withdrawing aliquots hourly and analyzing them in a Hewlett-Packard HP-6890 chromatograph. To corroborate product identification, the product mixture was analyzed in a HP GC–MS instrument (G 1800 B GCD system). Liquid yield was defined as the percent of liquid present at the end of the reaction with respect to the liquid in the feed.

3. Results and discussion

3.1. Catalyst characterization

The textural properties of the catalysts are shown in Table 1. For the sake of comparison, the total surface area values of the corresponding supports are also included in Table 1. Apparently, the area of the catalysts and their micropore area increase with zeolite loading in the support. However, a comparison of the surface areas of supports and catalysts reveals that the incorporation of the Ni and Mo phases caused an increasing loss in the total surface area, which can be due to a partial blocking of the zeolite micropores by oxidic Ni and Mo species. This is corroborated by the parallel decrease observed in micropore volume of the catalyst compared with the supports.

The XRD patterns of the oxidic catalysts are shown in Fig. 1. The γ-alumina diffraction lines are clearly observed and, as the zeolite content increases, diffraction lines attributed to faujasite begin to appear. There is no XRD evidence for the presence of crystalline MoO_3 and NiO phases, suggesting that such phases, if present, have crystal sizes smaller than 40 Å. The low intensity of the zeolite reflections in the alumina-zeolite-supported catalysts is due to the dilution effect caused by the presence of metals and the alumina matrix, and to the partial destruction of the zeolite framework resulting from the interaction with Mo and some dealuminization provoked by the acidic conditions during the peptizing process and Mo impregnation [13].

Table 1
Textural properties of supports and NiMo catalysts

Sample	S_{BET} (m^2/g)	S_μ (m^2/g)	V_p (cm^3/g)	V_μ (cm^3/g)	D_p (Å)
Al_2O_3	202	0	0.420	0.000	57
HNaY(5)-Al_2O_3	218	30	0.415	0.013	57
HNaY(10)-Al_2O_3	224	42	0.411	0.018	57
HNaY(20)-Al_2O_3	251	85	0.402	0.038	61
HNaY	696	593	0.361	0.276	37
NiMo/Al_2O_3	182	0	0.366	0.000	55
NiMo/HNaY(5)-Al_2O_3	190	21	0.348	0.008	55
NiMo/HNaY(10)-Al_2O_3	193	32	0.333	0.013	56
NiMo/HNaY(20)-Al_2O_3	196	49	0.312	0.022	59
NiMo/HNaY	239	189	0.118	0.088	37

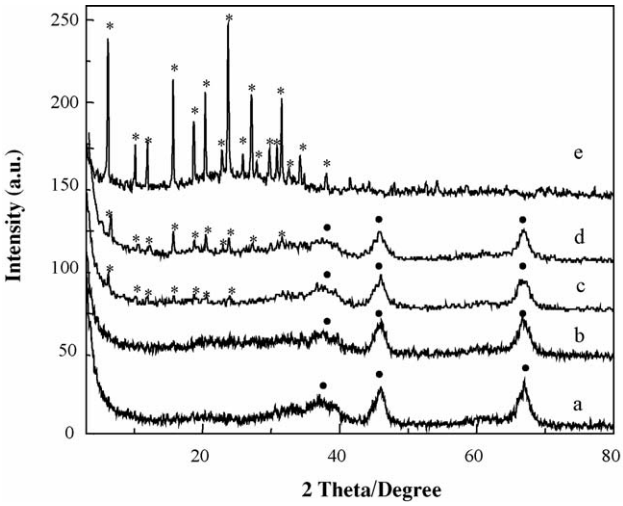

Fig. 1. X-ray diffraction patterns of NiMo catalysts supported on: (a) Al_2O_3, (b) HNaY(5)-Al_2O_3, (c) HNaY(10)-Al_2O_3, (d) HNaY(20)-Al_2O_3 and (e) HNaY. (*) Faujasite and (●) γ-Al_2O_3.

Fig. 2 presents the SEM-EDX line profiles of the oxidic NiMo/HNaY(20)-Al_2O_3 catalyst. A heterogeneous distribution of Ni and Mo in the catalyst is observed. The distribution of Mo follows that of Al while Ni shows no preference for Al or Si, suggesting that Mo was preferentially associated with alumina particles and in a minor proportion on zeolite, whereas Ni was deposited on both alumina and zeolite particles. These results are in agreement with those reported by Li et al. for Ni-Mo/γ-Al_2O_3-USY zeolite catalysts [17].

To identify the different metallic species present in the calcined catalysts, TPR experiments were made (Fig. 3). The TPR profile of the NiMo/Al_2O_3 (Fig. 3a) is typical of this type of catalysts [18]. It displays two principal reduction peaks

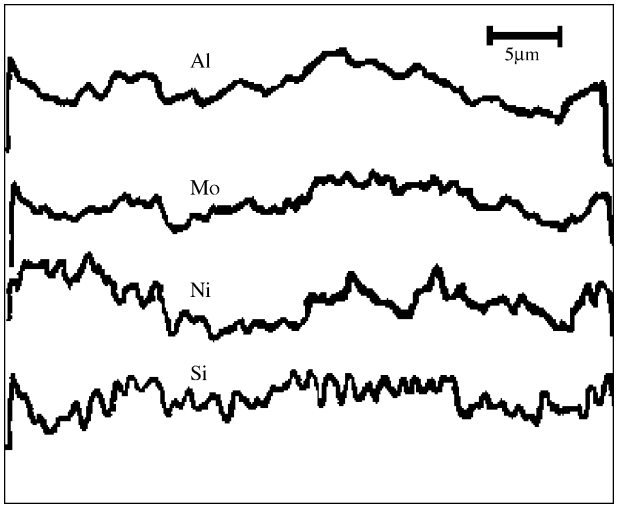

Fig. 2. SEM-EDX profile of NiMo/HNaY(20)-Al_2O_3 catalyst.

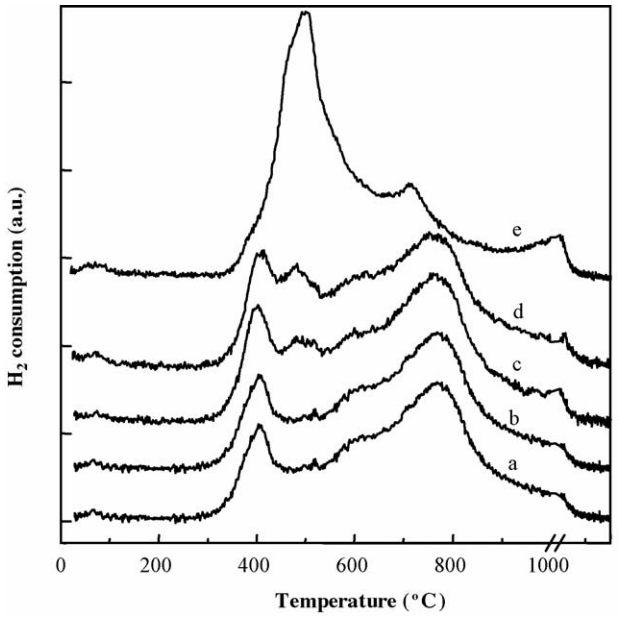

Fig. 3. TPR profiles of the NiMo catalysts supported on: (a) Al_2O_3, (b) HNaY(5)-Al_2O_3, (c) HNaY(10)-Al_2O_3, (d) HNaY(20)-Al_2O_3 and (e) HNaY. Isothermal period after the axis break.

where the first is located at about 425 °C, related to the first step of reduction $Mo^{6+} \rightarrow Mo^{4+}$ of the well dispersed octahedral Mo species, and the second one located at about 770 °C, which is related to the second step of reduction of the octahedral Mo species and to the first step of reduction of tetrahedral Mo species strongly bonded to the alumina support. In the TPR of the NiMo/Al_2O_3 catalyst the presence of octahedrally coordinated polymeric Mo and MoO_3 crystallites, which reduce in the region 450–570 °C [18], was not appreciable. The shoulder observed at about 600 °C could be assigned to the reduction of octahedrally coordinated Ni^{2+} species on the alumina surface. With the increase of zeolite content in catalyst support (Fig. 3b–d), a new peak at about 500 °C (assigned to polymeric octahedral Mo species supported on zeolite) increases and the peaks due to the reduction of well dispersed octahedral (425 °C) and tetrahedral Mo species (800 °C) decrease. These changes indicate that the amount of agglomerated octahedral Mo species increases at the expense of the dispersed tetrahedral species with increase of zeolite loading in the alumina matrix. These polymeric Mo species should be located on the zeolite component of the mixed support. This supposition is confirmed by considering the features of the TPR profile of the NiMo catalyst supported on pure HNaY (Fig. 3e). It shows two principal reduction peaks: the first one, very broad and more intense, is located at about 500 °C and can be assigned to polymeric octahedral Mo species on the zeolite surface, mostly located outside the zeolite cavities due to its low reduction temperature; and the second one at about 710 °C could be assigned to tetrahedrally coordinated Mo species in the zeolite cavities. This shift toward lower reduction temperature of tetrahedral Mo species

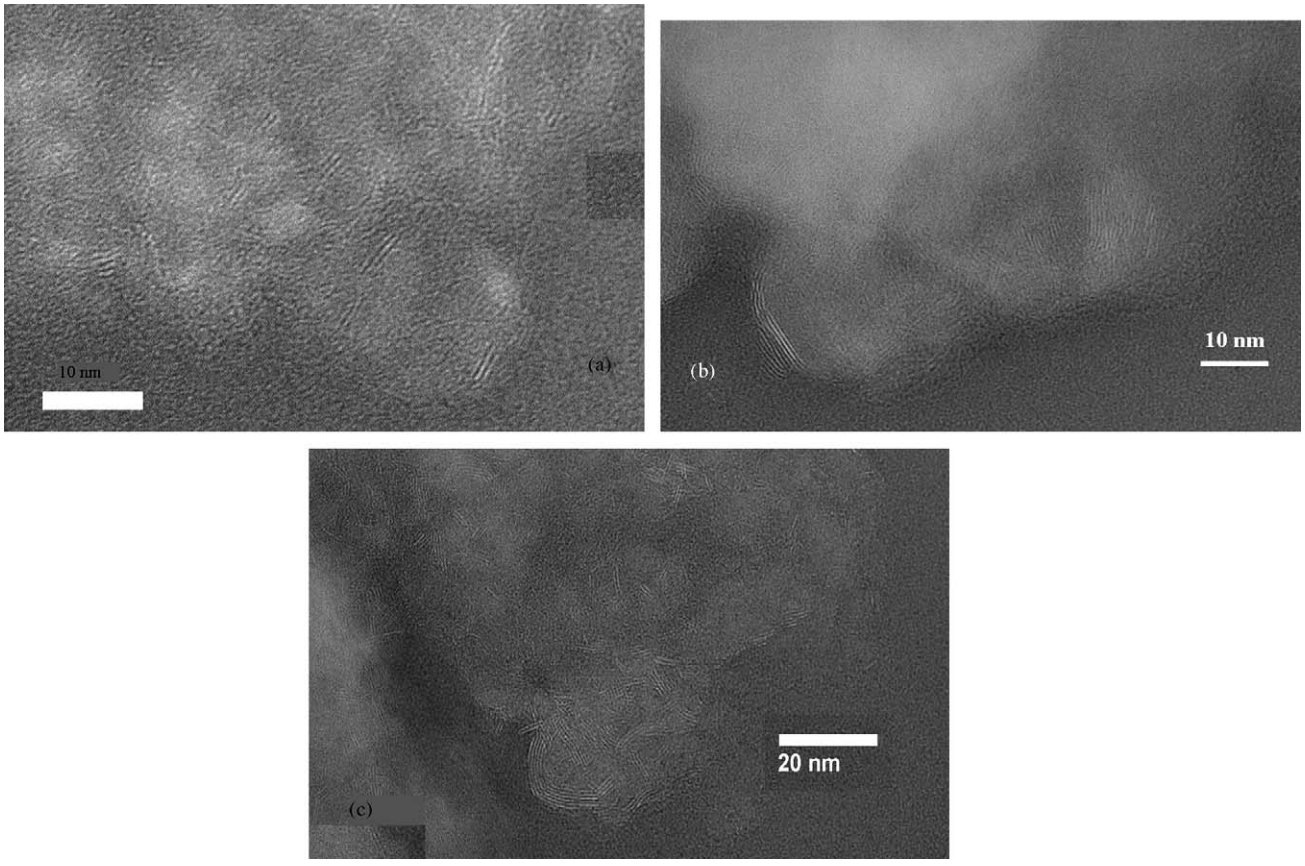

Fig. 4. HRTEM micrograph of sulfided: (a) NiMo/Al_2O_3 catalyst, (b) NiMo/HNaY catalyst and (c) NiMo/HNaY(20)-Al_2O_3catalyst.

is consistent with a weaker interaction of the oxide Mo species with the zeolite than with the alumina. In this catalyst, a defined reduction peak due to Ni^{2+} species was not observed, but in the temperature range 500–700 °C, the reduction of Ni^{2+} species was observed, depending on the Ni^{2+} location in the zeolite [14]. The peak of such species is probably masked by the broad, and intense peak located at 500 °C due to the Mo species.

The HRTEM micrographs of the sulfided $NiMo/Al_2O_3$, NiMo/HNaY and $NiMo/HNaY(20)-Al_2O_3$ are shown in Fig. 4a–c. The $NiMo/Al_2O_3$ displays MoS_2 crystallites with interplanar distances of 6.12 Å, with an average length of 33 Å and one to three slabs (Fig. 4a). In contrast, MoS_2 in NiMo/HNaY looks less disperse. The sample is mainly composed of large and highly stacked MoS_2 particles. MoS_2 crystallites with two to four stacked layers and an average length of 82 Å were observed in this case (Fig. 4b). As for the $NiMo/HNaY(20)-Al_2O_3$ intermediate values of average length (51 Å) and stacking of two to three slabs were observed (Fig. 4c). So, in line with the TPR results for the oxide precursors, the HRTEM micrographs show the increasing stacking and growing of the MoS_2 crystallites with the zeolite content.

According to the aforesaid, Fig. 5 shows that the amount of coordinatively unsaturated sites (CUS) of MoS_2 measured by the FT-IR/NO chemisorption on sulfided catalysts decreases pronouncedly with the increase in the zeolite content. This confirms that the dispersion of MoS_2 decreases markedly by increasing the zeolite content in the catalytic support. Fig. 5 shows also the results of acidity determined by the FT-IR of the Py thermo-desorption on oxidic catalysts. As expected, the concentration of the Brönsted acid sites (desorption temperature 250 °C) clearly increases with the amount of the zeolite incorporated into the alumina matrix. In this figure the behavior of both functionalities attributed to the molybdenum sulfide surface sites and zeolite Brönsted acid sites is compared. The catalysts display an opposite tendency for the acid and MoS_2 functions with the zeolite content in the support. Whereas the CUS number decreases, the number of strong Brönsted acid sites increases. This variation should have an important effect on the HDS of DBT and 4,6-DMDBT.

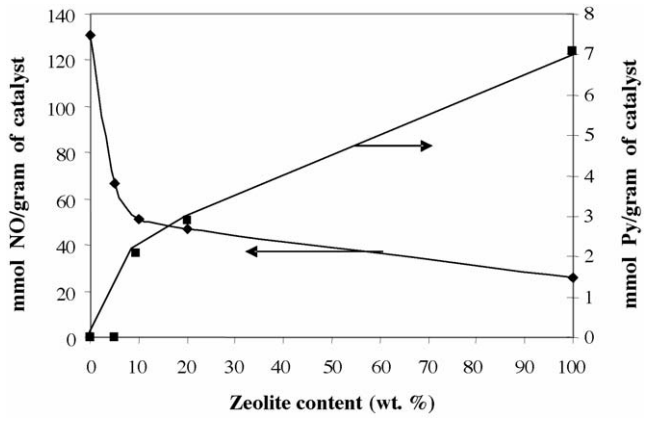

Fig. 5. Changes in CUS and Brönsted acid site concentrations in the NiMo catalysts with zeolite content in the support. Number of CUS was determined from IR of chemisorbed NO, and Brönsted acidity was calculated from Py-IR data obtained at 250 °C.

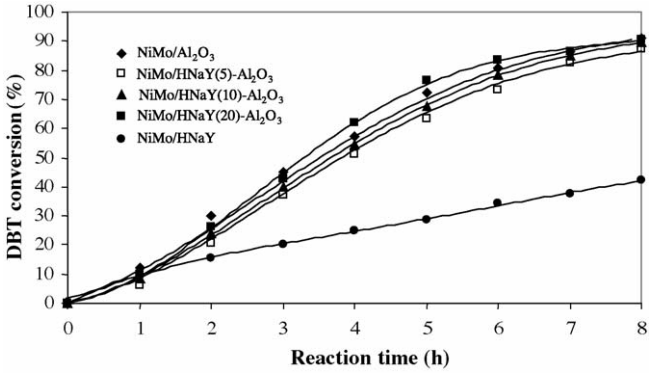

Fig. 6. DBT conversion obtained over $NiMo/HNaY(x)-Al_2O_3$.

3.2. Catalytic activity

3.2.1. Comparison of the total activities of the catalysts

Figs. 6 and 7 show the conversion with reaction time for DBT and 4,6-DMDBT, respectively, on the various catalysts. In order to compare the total activity of the catalysts, the initial reaction rate was calculated from the slope of the plots of DBT or 4,6-DMDBT conversion percent versus reaction time (Fig. 8). As expected, the initial activity of the $NiMo/Al_2O_3$ catalyst for the HDS of DBT was significantly higher (about six times) than for 4,6-DMDBT, as previously reported in the literature [2–4]. Fig. 8 shows that the incorporation of the HNaY zeolite to the support has somehow a different effect on the transformation of DBT compared to 4,6-DMDBT. With the incorporation of a small amount (5 wt.%) of zeolite into the support, the initial HDS rate of DBT decreased significantly (about 34%), while that of 4,6-DMDBT increased slightly (about 6%). The incorporation of further amounts of zeolite to the support led to a gradual increase in the initial HDS rate of both DBT and 4,6-DMDBT, as illustrated in Fig. 8. Note, however, that the NiMo catalysts containing high zeolite loading were significantly less active than the $NiMo/Al_2O_3$ in the HDS of the DBT and, on the contrary, more active in the conversion of 4,6-DMDBT. In general, this catalytic activity is in agreement with previous findings on zeolite-containing hydrotreating catalysts [2–12]. Furthermore, when the reaction time is long (>4 h) the activity trend described above changes

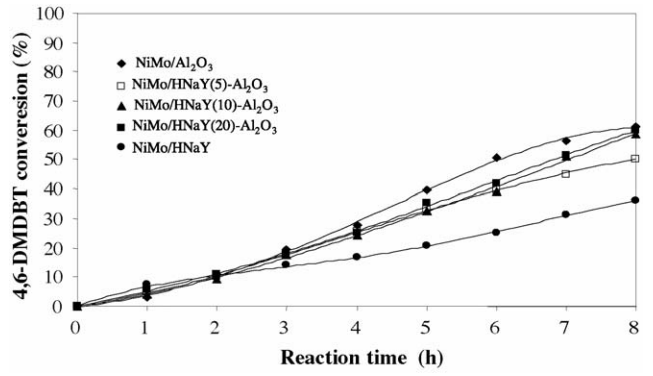

Fig. 7. 4,6-DMDBT conversion obtained over $NiMo/HNaY(x)-Al_2O_3$.

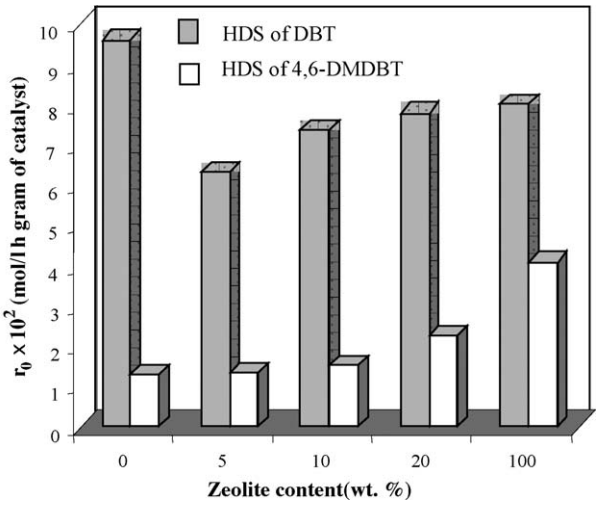

Fig. 8. Initial reaction rate HDS of DBT and 4,6-DMDBT over NiMo/HNaY(x)-Al_2O_3 catalysts with different zeolite loadings in the support.

(see Figs. 6 and 7) due to differences in catalyst deactivation. The zeolite-containing catalysts were deactivated significantly with reaction time as a result of coking on strong acid sites [3,10,15,19]. The amount of coke found in the spent catalysts was larger for the 4,6-DMDBT hydrodesulfurization tests, and increased significantly with zeolite loading (Table 2). The catalysts, which had larger amounts of coke, suffered quicker deactivation process. Therefore, it can be assumed that the changes in the catalytic activity with reaction time must be related to the susceptibility of the catalysts to form coke.

In order to explain the results mentioned above, it is necessary to take into account that: (i) the incorporation of the HNaY zeolite to the support leads, on one hand, to an important decrease in the amount of coordinatively unsaturated active sites on the MoS_2 surface as determined by NO adsorption and, on the other hand, a significant increase in the amount of Brönsted acid sites (Fig. 5); (ii) both types of active sites, metal sulfide and acidic, participate in the transformations of DBT and 4,6-DMDBT according to their reactivities through the different routes of hydrodesulfurization (DDS, HYD, ISO and CGK) [2–4,7]. Consequently, for the transformation of DBT it is expected that the decrease in the number of active sites (CUS) of the metal sulfide caused by zeolite incorporation would decrease the direct desulfurization route of DBT, which is the principal pathway for the transformation of this molecule [2–7,10]. At the same time, the increase in the number of acid sites would contribute to increase slightly the desulfurization of the DBT through the CKG route [7,19] and possibly to enhance the HYD route, as previously observed for Mo supported on HY zeolite [12]. This increase of the HDS activity of metal sulfides by acidic supports has been related, at least partly, to the improvement of their hydrogenation properties [7,9,10,12,20,21] and ascribed to electronic effects of the zeolite acidity on the supported phase [4,21–23]. Furthermore, Rozanska et al. reported recently that theoretical calculations indicate that pure zeolite alone can hydrodesulfurize DBT through both direct sulfur atom elimination and hydrogenation–desulfurization routes [24]. Thus, in Fig. 8, catalytic activity follows a combined trend determined by the two type of sites (Fig. 5), where at low zeolite content the global HDS activity drops due to the large decrease in metal active sites, while at high zeolite contents the total conversion of DBT increased due to the positive contribution of the reactions promoted indirectly [9,10,12,20] and/or directly [21–24] on the acid sites. In contrast, in the case of 4,6-DMDBT, Fig. 8 shows a positive effect of the zeolite content on the initial catalytic activity and the total 4,6-DMDBT conversion for all catalysts containing zeolite. In this case, it appears that the zeolite Brönsted acid

Table 2
Coke deposition on spent NiMo/HNaY(x)-Al_2O_3 catalysts

Catalyst	Coke (wt.%)	
	DBT HDS	4,6-DMDBT HDS
NiMo/Al_2O_3	1.1	1.6
NiMo/HNaY(5)-Al_2O_3	1.3	1.7
NiMo/HNaY(10)-Al_2O_3	1.7	2.2
NiMo/HNaY(20)-Al_2O_3	1.9	2.7
NiMo/HNaY	n.d.	n.d.

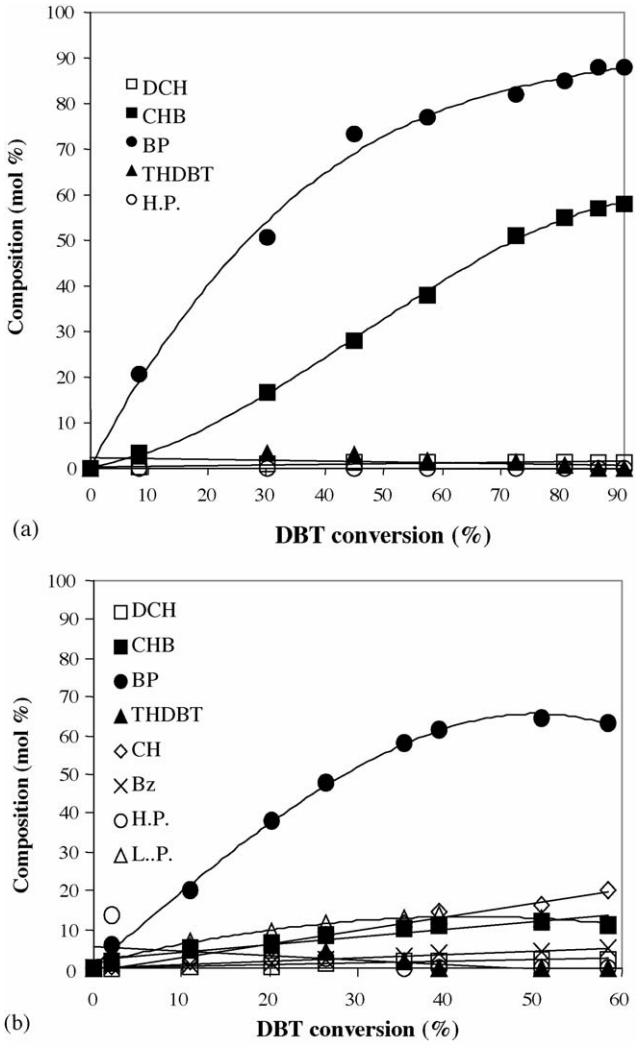

Fig. 9. Product distribution through conversion percent for hydrodesulfurization of DBT over NiMo/Al_2O_3 catalyst (a) and NiMo/HNaY(20)-Al_2O_3 (b).

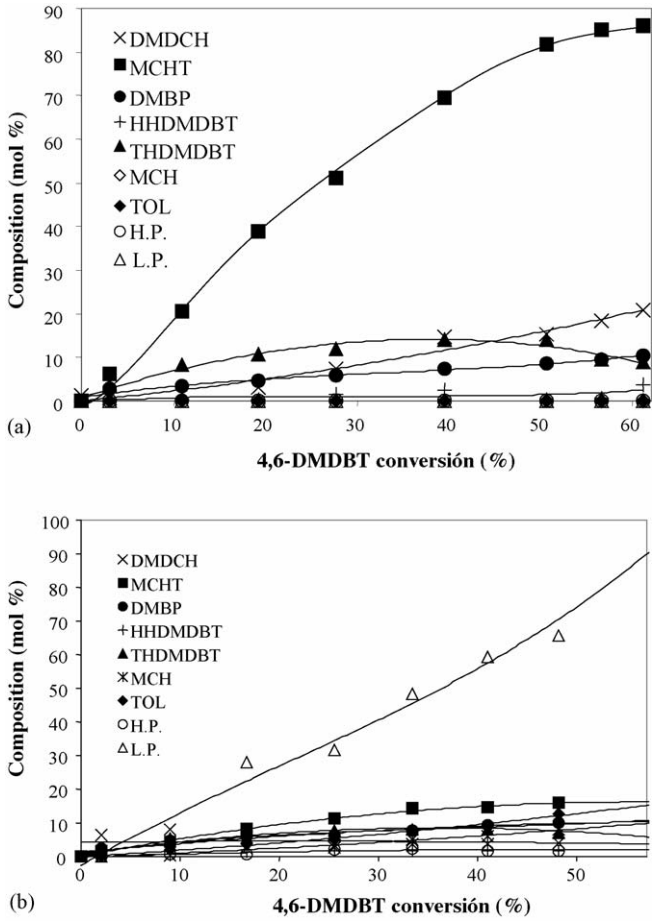

Fig. 10. Product distribution through conversion percent for hydrodesulfurization of 4,6-DMDBT over NiMo/Al_2O_3 catalyst (a) and NiMo/HNaY(20)-Al_2O_3 (b).

sites are able to promote significantly the ISO route and presumably also the HYD route for the hydrodesulfurization of 4,6-DMDBT, in addition to the CKG reactions of the desulfurized products [2–4,7,8]. Accordingly, higher concentration of products from the HYD, ISO and CKG reactions was observed in the final products.

3.2.2. Reaction product distribution

To enquire on the effect of HNaY zeolite on the transformation of DBT and 4,6-DMDBT, the reaction product distribution as a function of the total conversion was examined for both reactions over NiMo/Al_2O_3 and NiMo/HNaY(20)-Al_2O_3 (Figs. 9 and 10).

As Table 3 shows, over NiMo/Al_2O_3, DBT was transformed only through the two expected routes (DDS and HYD), giving mainly biphenyl (BP) and in minor amount cyclohexylbenzene (CHB) as the reaction products (Fig. 9a) resulting from the DDS and HYD routes, respectively, in agreement with the literature [2–4]. For 4,6-DMDBT on NiMo/Al_2O_3, the HYD and DDS routes are also the main routes, but HYD being the predominant pathway for this case. No evidence of cracking, light or heavy products (Fig. 10a) was found when this catalyst was used.

Over NiMo/Al_2O_3-HNaY(20), for the HDS of DBT the main route is also the DDS, giving BP as the major product (see Table 3). However, benzene, cyclohexane, heavy and especially light products appear in significant concentrations as Table 3 and Fig. 9b show. It is well known that these products result from the cracking route of DBT and its HDS products on the Brönsted acid sites of the HNaY zeolite [4,8].

The transformation of 4,6-DMDBT over NiMo/Al_2O_3-HNaY(20) yields products from the isomerization, cracking and alkylation reaction routes (see Table 4 and Fig. 10b). We observe a high quantity of light products (C_4–C_6), which increases with conversion. Toluene and methylcyclohexane are produced through cracking of methylcyclohexyltoluene.

Summarizing, Tables 3 and 4 show a comparison of the product distributions of all catalysts at the same conversion of DBT and 4,6-DMDBT (about 35%), respectively. In the case of DBT (Table 3), the two major products, biphenyl (DDS route) and cyclohexylbenzene (HYD route), decrease significantly with zeolite content in the support, increasing benzene, cyclohexane and heavy and light products (C_4–C_6) formed by cracking and hydrocracking reactions. At high zeolite content (20%) the loss of liquid yield (defined before) reflects the high amount of light products formed. Significant amounts of heavy compounds, such as mono- and polyalkylated DBT's

Table 3
Liquid yields and reaction product compositions obtained over NiMo/HNaY(x)-Al_2O_3 catalysts at 35% of total DBT conversion

Product	Catalyst				
	NiMo/Al_2O_3	NiMo/HNaY(5)-Al_2O_3	NiMo/HNaY(10)-Al_2O_3	NiMo/HNaY(20)-Al_2O_3	NiMo/HNaY
THDBT	3.27	3.62	3.69	4.00	4.86
BP	69.95	72.21	71.10	67.10	14.73
CHB	26.65	23.53	13.20	10.06	3.15
DCH	1.09	0.67	–	–	3.52
CH	–	0.64	0.90	1.50	1.69
BZ	–	–	1.70	2.46	0.53
L.P.	–	–	8.00	12.0	23.53
H.P.	–	–	1.10	3.33	47.97
Liquid yield (%)	100	96.1	90.9	88.1	85.7

BP, biphenyl; CHB, cyclohexylbenzene; DCH, dicyclohexyl; CH, cyclohexane; BZ, benzene; L.P., light products (C_4–C_6); H.P., heavy products obtained from DBT alkylation.

Table 4
Liquid yields and reaction product compositions obtained over NiMo/HNaY(x)-Al_2O_3 catalysts at 35% of total 4,6-DMDBT conversion

Product	Catalyst				
	NiMo/Al_2O_3	NiMo/HNaY(5)-Al_2O_3	NiMo/HNaY(10)-Al_2O_3	NiMo/HNaY(20)-Al_2O_3	NiMo/HnaY
THDMDBT	12.4	9.89	8.85	8.42	5.94
HHDMDBT	2.47	2.12	2.60	1.89	0.86
DMBP	7.54	8.07	8.55	7.68	12.54
MCHT	63.49	62.12	28.24	14.26	4.03
DMDCH	14.01	8.04	7.83	4.53	–
TL	–	6.03	6.56	7.59	7.53
MCH	–	3.73	10.45	4.99	7.22
H.P.	–	–	1.14	2.43	21.54
L.P.	–	–	25.78	49.93	40.34
Liquid yield (%)	96.6	96.1	94.3	92.8	83.1

THDMDBT, tetrahydrodimethyldibenzotiophene; HHDMDBT, hexahydrodimethyldibenzotiophene; DMBP, dimethylbiphenyl; MCHT, methylcyclohexyltoluene; DMDCH, dimethyldicyclohexyl; TL, toluene; MCH, methylcyclohexane; L.P., light products (C_4–C_6); H.P., heavy products from alkylation of the 4,6-DMDBT.

or biphenyls and light compounds were detected for the catalyst supported on pure zeolite (Table 3) like the main products.

Indeed, Table 4 shows that the product distribution of HDS of 4,6-DMDBT over NiMo/Al_2O_3 yielded predominantly methycyclohexyltoluene and dimethyldicyclohexyl (HYD route products) and to a minor extent of dimethylbiphenyl (DDS route). With the incorporation of zeolite to the catalyst, the production of hydrogenated products is still predominant respect to those formed through DDS. An increase of light products (toluene, methylcyclohexane and C_4–C_6) results from the cracking of MCHT, DMDCH and DMBP. Some unidentified heavier products than 4,6-DMDBT were observed. In line with this, a higher amount of coke was found in the zeolite-containing catalysts used in the transformation of 4,6-DMDBT (see Table 2). The formation of different isomers of methycyclohexyltoluene and dimethyldicyclohexyl increased with content of zeolite, except for the NiMo/HNaY catalyst, where the DMBP concentration in the product is higher than that of MCHT. The possible cause for this is the fast transformation of MCHT to cracking products. Accordingly, light and heavy products, such as mono- and polyalkylated DBT's or biphenyls, are observed as the main products.

These results indicate that to achieve a high efficiency for the HDS of DBT the CUS have higher importance than the Brönsted acid sites. The possible electronic effect of the acid sites on the reactivity of DBT is relatively small [8,21,22]. For the HDS of 4,6-DMDBT are, however, necessary the participation of both types of sites, the CUS of the MoS_2 phase and the Brönsted acid sites of the zeolite. The role of the Brönsted acid sites is to change the molecule in another more reactive either by isomerization or demethylation and thus alleviate the steric hindrance effect [2–4]. Such a positive effect of the acid sites of zeolite on catalytic activity was shown in the present work by the presence of almost eight different isomers of MCHT, which were grouped like the same compound in Table 4. As previously reported in the literature [4,8,21,22], the contribution also of the acid sites to the HDS of 4,6-DMDBT through the HYD route, by improving the hydrogenation activity of the sulfide phase, is probably very important in this case, although there are not proofs for this route due probably to the rapid cracking of the MCHT into toluene and methylcyclohexane [2,4,7,12].

From those results, it can be concluded that in the case of 4,6-DMDBT, the addition of the zeolite acid function to the catalyst support leads to a higher overall HDS catalytic activity than that exhibited for the conventional alumina-supported counterpart. The increase in HDS reactivity of 4,6-DMDBT is due to its transformation in other more reactive compound through isomerization, demethylation and hydrogenation reactions promoted by the acid sites of the zeolite. But the presence of strong acid sites in the HNaY zeolite leads also to cracking reactions and deactivation by coking. However, this effect can be diminished to acceptable values, adjusting the content of zeolite in catalyst or changing Si/Al ratio [8,25]. Therefore, further research will be necessary to optimize the zeolite acidity for limiting undesirable side reactions and coking.

4. Conclusions

For NiMo catalysts supported on HNaY(x)-Al_2O_3, an augment of zeolite content leads to an increase in Brönsted acid sites and, on the other hand, to an increase in the proportion of polymeric octahedrally coordinated Mo species. This gave rise consequently to an increase in the crystallite size of MoS_2 and to a decrease in the number of coordinatively unsaturated sites. Thus, the change in support composition changes the relation between metallic and acid functionalities, causing significant differences in catalytic performance.

The effect of the zeolite content on the HDS of DBT was small, because the transformation of this molecule occurs essentially through the DDS and HYD routes over the metal sulfided phases, and the acid sites do not contribute to a better catalytic performance. In contrast, for 4,6-DMDBT HDS, there is an important contribution of the zeolite acid sites through acid-catalyzed isomerization, cracking and disproportionation or trans-alkylation reactions of the, 4,6-DMDBT, yielding non-sterically hindered compounds that desulfurize easier by the DSD route on the sulfided phase.

Acknowledgements

The authors acknowledge financial support from the DGAPA-UNAM, México, Project IN-103102, and the DGICyT, Ministry of Science and Technology, Spain, Project BQU2001-2126. We would like to thank Ivan Puente-Lee for obtaining the HRTEM micrographs and Cecilia Salcedo-Luna for help with XRD characterizations.

References

[1] R. Shafi, G.J. Hutchings, Catal. Today 59 (2000) 423.
[2] P. Michaud, J.L. Lemberton, G. Pérot, Appl. Catal. A: Gen. 169 (1998) 343.
[3] D.D. Withehurst, T. Isoda, I. Mochida, Adv. Catal. 42 (1998) 345.
[4] G. Perot, Catal. Today 86 (2003) 111.
[5] T. Isoda, S. Nagao, X.L. Ma, Y. Korai, I. Mochida, Energy Fuels 10 (1996) 1078.
[6] C. Kwak, J. Joon Lee, J. Sang Bae, K. Choi, S. Heup Moon, Appl. Catal. 200 (2000) 233.
[7] M.V. Landau, D. Berger, M. Herskowitz, J. Catal. 159 (1996) 236.
[8] N. Kunisada, K. Choi, Y. Korai, I. Mochida, K. Nakano, Appl. Catal. A: Gen. 276 (2004) 51.
[9] E. Lecrenay, I. Mochida, Stud. Surf. Sci. Catal. 106 (1997) 333.
[10] E. Lecrenay, K. Sakanishi, I. Mochida, Catal. Today 39 (1997) 13.
[11] D. Li, A. Nishijima, D.E. Morris, J. Catal. 182 (1999) 339.
[12] F. Bataille, J.L. Lemberton, G. Pérot, P. Leyrit, T. Cseri, N. Marchal, S. Kasztelan, Appl. Catal. A: Gen. 220 (2001) 191.
[13] T. Klimova, D. Solís, J. Ramírez, A. López-Agudo, Stud. Surf. Sci. Catal. 143 (2002) 267.
[14] R. Cid, J. Neira, J. Godoy, J.M. Palacios, A. López Agudo, Appl. Catal. A 125 (1995) 169.
[15] D. Solís, T. Klimova, R. Cuevas, J. Ramírez, A. López Agudo, Catal. Today 98 (2004) 201.
[16] T. Klimova, D. Solís, J. Ramírez, A. López Agudo, Stud. Surf. Sci. Catal. 127 (1999) 373.
[17] D. Li, A. Nishijima, D.E. Morris, G.D. Guthrie, J. Catal. 188 (1999) 111.
[18] R. López Cordero, A. López Agudo, Appl. Catal. A 202 (2000) 23.
[19] W.J.J. Welters, V.H.J. de Beer, R.A. van Santen, Appl. Catal. A 119 (1994) 253.
[20] P. Leyrit, T. Cseri, N. Marchal, J. Lynch, S. Kasztelan, Catal. Today 65 (2001) 249.
[21] E. Lecrenay, K. Sakanishi, T. Nagamatsu, I. Mochida, T. Suzki, Appl. Catal. B: Environ. 18 (1998) 325.
[22] M. Breysse, P. Afanasiev, C. Geantet, M. Vrinat, Appl. Catal. 86 (2003) 5.
[23] M.J. Vissenberg, P.W. de Bont, W. Gruitjers, V.J.H. de Beer, A.M. van der Kraan, R.A. van Santen, J.A.R. Van Veen, J. Catal. 189 (2000) 209.
[24] X. Rozanska, X. Saintigny, R.A. van Santen, S. Clemendot, F. Hutschka, J. Catal. 208 (2002) 89.
[25] C. Marín, J. Escobar, E. Galván, F. Murrieta, R. Zárate, H. Vaca, Fuel Process. Technol. 86 (2004) 391.